Journal of
Composites Science

MDPI

Communication

The Benefit of the Glassy State of Reinforcing Particles for the Densification of Aluminum Matrix Composites

Vyacheslav I. Kvashnin [1,2], Dina V. Dudina [1,2,3,*], Arina V. Ukhina [3], Guilherme Yuuki Koga [4] and Konstantinos Georgarakis [5,*]

[1] Lavrentyev Institute of Hydrodynamics SB RAS, Lavrentyev Ave. 15, 630090 Novosibirsk, Russia; slava.kvashnin@mail.ru
[2] Department of Mechanical Engineering, Novosibirsk State Technical University, K. Marx Ave. 20, 630073 Novosibirsk, Russia
[3] Institute of Solid State Chemistry and Mechanochemistry SB RAS, Kutateladze Str. 18, 630128 Novosibirsk, Russia; auhina181@gmail.com
[4] Department of Materials Science and Engineering, Federal University of São Carlos, Via Washington Luiz, km 235, São Carlos 13565-905, SP, Brazil; guilherme.koga@gmail.com
[5] School of Aerospace, Transport and Manufacturing, Cranfield University, Cranfield MK43 0AL, UK
* Correspondence: dina1807@gmail.com (D.V.D.); k.georgarakis@cranfield.ac.uk (K.G.)

Abstract: In metallic glass-reinforced metal matrix composites, the glassy phase can serve a dual purpose: (i) it can behave as soft binder and porosity remover during consolidation; and (ii) it can act as the hard reinforcing phase after densification. The present work aimed to demonstrate the benefit of the glassy reinforcing particles for the densification of aluminum matrix composites. The consolidation behavior of Al–50 vol.% Fe-based alloy mixtures prepared using a glassy $Fe_{66}Cr_{10}Nb_5B_{19}$ alloy powder (T_g = 521 °C, T_x = 573 °C) or a crystalline $Fe_{62}Cr_{10}Nb_{12}B_{16}$ alloy powder was studied under spark plasma sintering (SPS) and hot pressing (HP) conditions. The powders were consolidated by heating above the glass transition temperature of the glassy alloy (up to 540 °C in SPS and 570 °C in HP). When the coarse aluminum powder was used, the reinforcing particles formed chains within the microstructure. In composites formed from the fine Al powder, the particles of the Fe-based alloy were separated from each other by the metallic matrix, and the tendency to form agglomerates was reduced. The glassy state of the alloy was shown to be beneficial for densification, as the metallic glass acted as a soft binder. The densification enhancement effect was more pronounced in the case of reinforcing particles forming chains. The hardness of the Al–50 vol.% glassy $Fe_{66}Cr_{10}Nb_5B_{19}$ composites obtained by SPS was twice the hardness of the unreinforced sintered aluminum (110 HV_1 versus 45 HV_1).

Keywords: aluminum matrix composite; spark plasma sintering; hot pressing; microstructure; metallic glass; reinforcement

Citation: Kvashnin, V.I.; Dudina, D.V.; Ukhina, A.V.; Koga, G.Y.; Georgarakis, K. The Benefit of the Glassy State of Reinforcing Particles for the Densification of Aluminum Matrix Composites. *J. Compos. Sci.* **2022**, *6*, 135. https://doi.org/10.3390/jcs6050135

Academic Editors: Oscar Marcelo Suárez and Hongseok Choi

Received: 5 April 2022
Accepted: 5 May 2022
Published: 7 May 2022

1. Introduction

Metal matrix composites present a broad class of materials, as numerous matrix-reinforcement combinations are possible. Aluminum matrix composites have attracted particular attention owing to their high specific strength [1,2]. The traditional approach to obtaining these composites is to introduce ceramic particles as a reinforcing phase [3,4]. Despite commercial availability and chemical inertness of ceramic materials, ceramic particle-reinforced aluminum matrix composites can suffer from weak interfaces and agglomeration of ceramic particles causing the formation of difficult-to-eliminate porosity within the agglomerates [5].

An alternative approach to reinforcing aluminum is to add phases/particles of metallic nature to form strong bonding at the matrix/reinforcement interface. Along this line, particles of high-entropy [6,7] or quasicrystalline alloys [8,9] can act as reinforcements. An

attractive possibility is to use glassy alloys for reinforcing aluminum. Metallic glasses are known for their high hardness, high strength, and an elastic strain limit of ~2% [10–12]. They behave as viscous liquids above their glass transition temperature. In the supercooled liquid region, the viscosity of the material drops significantly allowing for shape changes under low stresses [13,14]. Upon cooling below the glass transition temperature, metallic glasses regain their hardness and strength. A decrease in viscosity can be used to advantage for obtaining dense aluminum matrix composites by powder consolidation, the metallic glass acting as both a binder and a reinforcing component [15]. Al–metallic glass composites have been obtained by hot rolling [16,17], hot pressing [18], hot extrusion [19], induction heating [15], hot pressing and subsequent hot extrusion [20,21], and spark plasma sintering (SPS) [22–24]. It is assumed that the application of external pressure helps deform the glassy particles and break the oxide films on the surfaces of the aluminum particles.

In the present work, we show the benefit of the glassy state of the added reinforcement for densification of aluminum matrix composites. The formation of composites from the Al–50 vol.% Fe-based alloy mixtures prepared using a glassy $Fe_{66}Cr_{10}Nb_5B_{19}$ alloy powder or a crystalline $Fe_{62}Cr_{10}Nb_{12}B_{16}$ alloy powder of the same size (20–40 μm fraction) was investigated. By selecting aluminum powders differing in size, we established different patterns of distribution of the alloy particles in the composites.

2. Materials and Methods

Al powders of two grades (PAD-6 grade, 99.9% purity, particle size range 3–10 μm and PA-4 grade, 98% purity, particle size range 10–45 μm) were used. A glassy $Fe_{66}Cr_{10}Nb_5B_{19}$ powder or a crystalline $Fe_{62}Cr_{10}Nb_{12}B_{16}$ powder having the same particle size range (20–40 μm) was added as a reinforcing component. For preparing the alloys, the following commercial purity materials were used: Fe-B alloy (B content 16.54 wt.%, ACL Metais, Araçariguama, Brazil), Fe-Nb alloy (Nb content 66.4 wt.%, ACL Metais, Araçariguama, Brazil), metallic chromium (Cr content > 99.3 wt.%, ACL Metais, Araçariguama, Brazil), and metallic iron (Fe content > 99.5 wt.%, Höganäs, Mogi das Cruzes, Brazil). The powders were obtained by argon gas atomization using a HERMIGA 75/5VI gas atomizer (Phoenix Scientific Industries Ltd., Hailsham, East Sussex, UK). The target fraction of the powders was separated by sieving.

The glass transition and crystallization temperatures of the $Fe_{66}Cr_{10}Nb_5B_{19}$ alloy are T_g = 521 °C and T_x = 573 °C (measured at a heating rate of 10° min^{-1}) [25].

The pycnometer density of the $Fe_{66}Cr_{10}Nb_5B_{19}$ and $Fe_{62}Cr_{10}Nb_{12}B_{16}$ powders is 7.58 g cm^{-3} and 7.62 g cm^{-3}, respectively.

The Al–Fe-based alloy mixtures containing 50 vol.% of Al were prepared by mixing the components in a mortar.

The mixtures were consolidated by SPS in a Labox 1575 apparatus (SINTER LAND Inc., Nagaoka, Japan) under a uniaxial pressure of 40 MPa. The powder mixture (weight: 1.5 g) was placed in a cylindrical graphite die of 10 mm internal diameter. Tungsten punches were used. A graphite foil lined the inner wall of the die and was also placed between the flat ends of the sample and the flat ends of the punches to prevent a direct interaction of the die and punch materials with the powder. Sintering was conducted in a forevacuum by means of heating up to 540 °C at an average rate of 50 °C min^{-1}.

Additional experiments were carried out using a hot press (a custom-made facility developed by the Institute of Automation and Electrometry SB RAS, Novosibirsk, Russia). Hot pressing (HP) was conducted in an argon atmosphere at a uniaxial pressure of 40 MPa by means of heating up to 570 °C at a rate of 50 °C min^{-1}.

After the graphite foil has been removed from the surface of the consolidated samples, their dimensions were accurately measured for calculating their volume and density.

SPS of the Fe-based alloy powders (not mixed with aluminum) was conducted to demonstrate the differences in the shrinkage behavior of the two alloys upon heating up to 540 °C. The displacement curves of the samples recorded during sintering have been analyzed.

The X-ray diffraction (XRD) patterns of the powders and sintered composites were recorded by a D8 ADVANCE diffractometer (Bruker AXS, Karlsruhe, Germany) using Cu Kα radiation. The morphology of the powders and microstructure of the sintered composites were studied by scanning electron microscopy using a LEO 420 microscope (Zeiss, Jena, Germany) and a TM-1000 Tabletop microscope (Hitachi, Tokyo, Japan). The images of the polished cross-sections of the sintered specimens were recorded in the secondary electron imaging (SE) mode. The images of the fracture surface of the samples were recorded in the back-scattered electron (BSE) mode.

Vickers hardness measurements were carried out on DuraScan 50 hardness tester (EMCO-TEST, Kuchl, Austria) at a load of 1 kg. The indentation direction was normal to the pressing direction during consolidation. An average hardness was determined from 9 measurements. Standard deviations are reported along with the average values.

3. Results and Discussion

3.1. Characteristics of the Aluminum and Fe-Based Alloy Powders

The morphology of the aluminum and Fe-based alloy powders used in the present work is shown in Figures 1 and 2, respectively. The two aluminum powders differ in the particle size. The powders are of spherical (or nearly spherical) shape. The XRD patterns of the Fe-based alloy powders are presented in Figure 3. The $Fe_{66}Cr_{10}Nb_5B_{19}$ alloy is mainly amorphous, while the $Fe_{62}Cr_{10}Nb_{12}B_{16}$ alloy is fully crystalline.

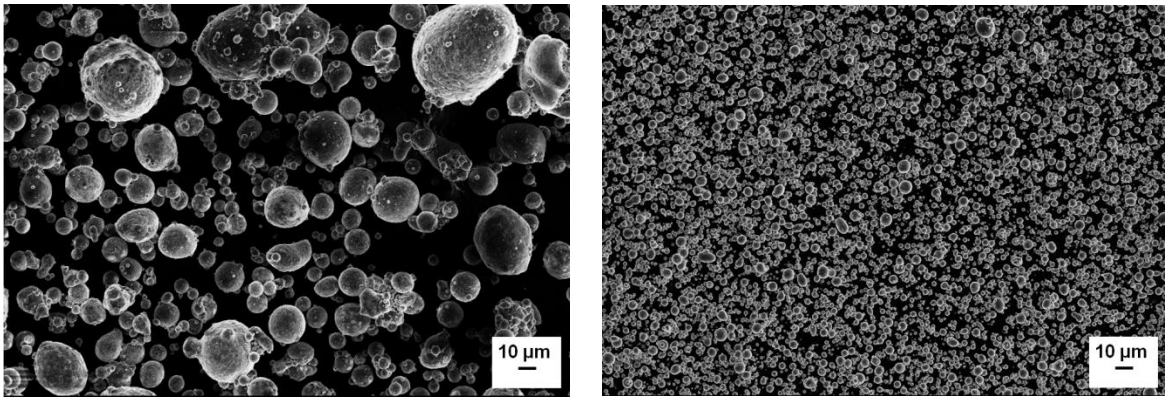

(**a**) (**b**)

Figure 1. Morphology of the Al powders: (**a**) coarse and (**b**) fine.

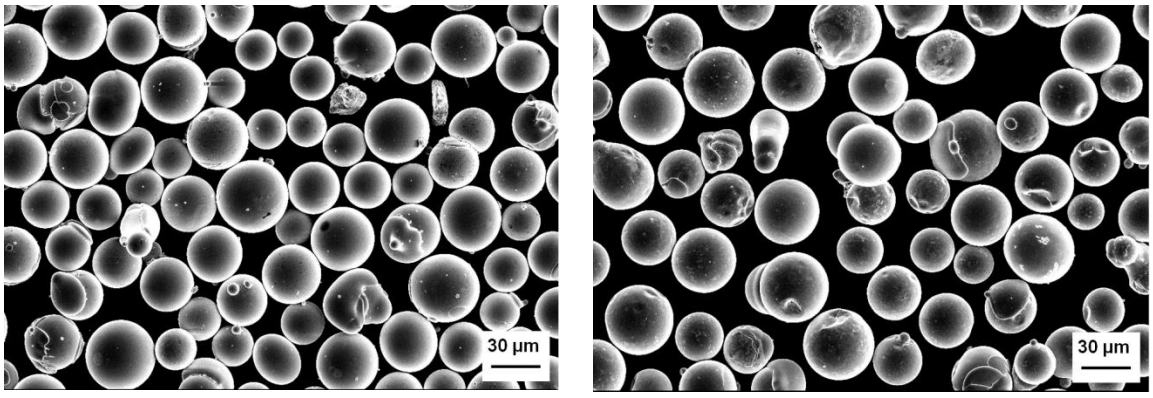

(**a**) (**b**)

Figure 2. Morphology of the Fe-based alloy powders: (**a**) glassy $Fe_{66}Cr_{10}Nb_5B_{19}$ and (**b**) crystalline $Fe_{62}Cr_{10}Nb_{12}B_{16}$ (20–40 µm fraction).

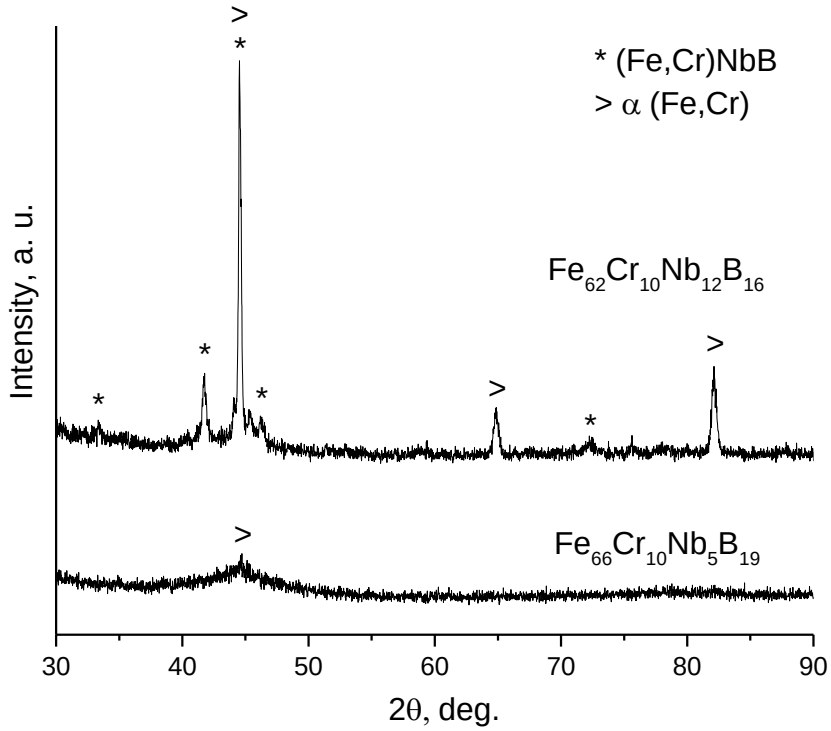

Figure 3. XRD patterns of the glassy $Fe_{66}Cr_{10}Nb_5B_{19}$ alloy and crystalline $Fe_{62}Cr_{10}Nb_{12}B_{16}$ alloy powders. (Fe,Cr)NbB has a hexagonal structure (space group $P\bar{6}2m$).

3.2. Structural Characteristics of the Sintered Composites

The XRD patterns of the sintered composites are presented in Figure 4. In the patterns of the composites formed from the coarse aluminum powder, the diffraction halo originating from $Fe_{66}Cr_{10}Nb_5B_{19}$ and reflections originating from $Fe_{62}Cr_{10}Nb_{12}B_{16}$ are weak (Figure 4a,b). The penetration depth of X-rays in the Fe-based alloys is much smaller than in aluminum (for the analysis conducted, it is smaller than the particle size of the alloys), so the diffracted intensity does not "correspond" to the real concentrations of the components in the composites. The X-rays allow detecting the very first layer only (when hitting the Fe-based particles directly) or two layers (aluminum and the alloy particle located underneath).

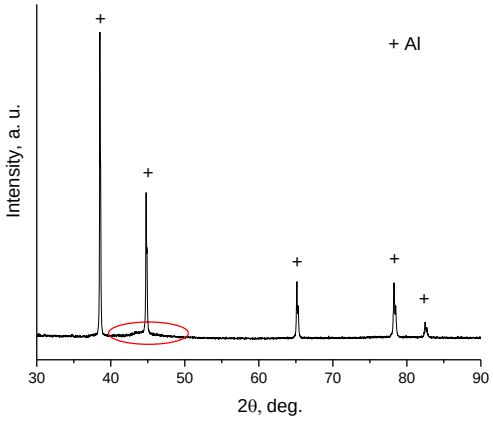

(**a**)

Figure 4. *Cont.*

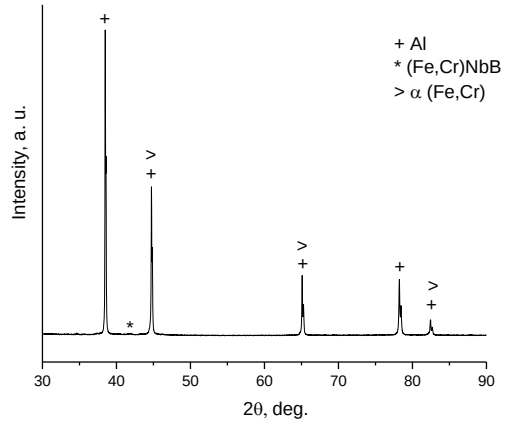

(**b**)

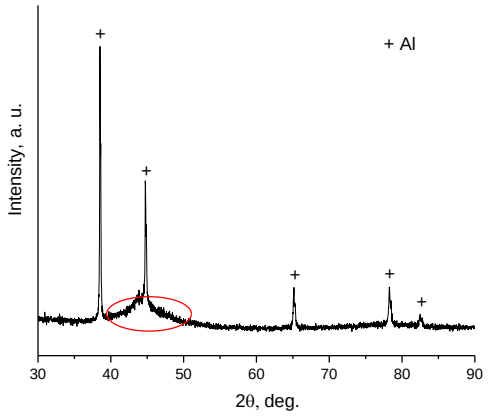

(**c**)

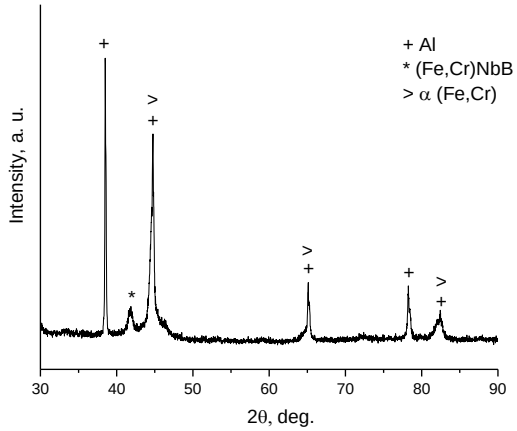

(**d**)

Figure 4. XRD patterns of the spark plasma sintered composites obtained from (**a**) Al (coarse)–glassy $Fe_{66}Cr_{10}Nb_5B_{19}$; (**b**) Al (coarse)–crystalline $Fe_{62}Cr_{10}Nb_{12}B_{16}$; (**c**) Al (fine)–glassy $Fe_{66}Cr_{10}Nb_5B_{19}$; and (**d**) Al (fine)–crystalline $Fe_{62}Cr_{10}Nb_{12}B_{16}$ mixtures. A red oval in (**a**,**c**) marks the range, in which a diffraction halo is present.

The fine aluminum powder can form thin layers in the subsurface region of the sample subjected to the analysis. When composites are made using the fine aluminum powder, the concentration of aluminum "detected" is lower than in the case of composites made from the coarse powder. In the patterns of the composites obtained using the fine aluminum powder, the evidence of the presence of the Fe-based alloys is clearly observed (Figure 4c,d). The XRD pattern of the composite sintered from the Al (fine)–glassy $Fe_{66}Cr_{10}Nb_5B_{19}$ shows a diffraction halo in the 42–48° (2θ) range, confirming the preservation of the amorphous phase in the consolidated state. In the pattern of the composite sintered from the Al (fine)–crystalline $Fe_{62}Cr_{10}Nb_{12}B_{16}$ mixture, a line corresponding to one of the crystalline phases of the alloy ((Fe,Cr)NbB) is clearly seen. Other lines of the crystalline phases overlap with reflections of aluminum. As seen from the XRD patterns of the composites, no significant chemical interaction between aluminum and the alloys occurred during consolidation.

The temperature of the HP experiments was deliberately taken higher than the measured temperature during SPS. This was done to make up for the difference in the samples' real temperature caused by the mode of heating. The temperature of the conductive specimens is always higher than the temperature of the die wall; in the case of relatively low sintering temperatures, the difference is several tens of degrees [26]. In the SPS process, local overheating effects at the inter-particle contacts can play a significant role in densification. So, the heating conditions are intrinsically different in these two consolidation processes. The XRD phase analysis did not reveal any reaction products in the hot-pressed composites (Figure 5).

Table 1 shows the relative densities of the composites. The theoretical density of the composites was calculated using the rule of mixtures and the density values of monolithic aluminum and the pycnometer density of the alloy powders. It is seen that densification of the Al (coarse)–glassy $Fe_{66}Cr_{10}Nb_5B_{19}$ powder mixture was more efficient than densification of the Al (coarse)–crystalline $Fe_{62}Cr_{10}Nb_{12}B_{16}$ mixture. So, if the glassy alloy powder is replaced by a crystalline alloy of close composition and the same particle size, the relative density of the composite drops down significantly, from 99% to 84%. The same effect is observed when composites are produced by HP, with the relative density values being lower (94% and 78%). Mixtures containing the fine aluminum powder densify efficiently, with only a smaller difference in the relative density between the composites containing the glassy and the crystalline alloy (99% versus 94%). From the analysis of the relative densities, it can be deduced that the state of the alloy (glassy/crystalline) plays a significant role in the densification process, the presence of a glassy alloy greatly enhancing densification. When the coarse aluminum powder is used for composing the mixtures, the effect is more pronounced.

The microstructural studies helped rationalize the observed differences in the relative densities. In the microstructure of the composite obtained from the Al (coarse)–$Fe_{66}Cr_{10}Nb_5B_{19}$ mixture (Figure 6a), particles of $Fe_{66}Cr_{10}Nb_5B_{19}$ contacted each other and formed chains. Within a chain, they sintered together, as the glassy alloy entered the supercooled liquid region. A high residual porosity of the composite sintered from the Al (coarse)–crystalline $Fe_{62}Cr_{10}Nb_{12}B_{16}$ mixture did not allow preparing a polished sample for microstructural observations. For this reason, we show a micrograph of the fracture surface of that sample (Figure 6b). Chains of crystalline $Fe_{62}Cr_{10}Nb_{12}B_{16}$ particles formed during sintering in a similar manner, but no inter-particle sintering occurred, as the crystalline alloy was not capable of reducing viscosity under the selected sintering conditions. In Figure 6a, it is seen that some particles detached from the matrix during polishing due to weak bonding at the interface. As shown in refs. [27–29], chemical reactions between the metal matrix and the metallic glass reinforcement result in the formation of intermetallic layers, which increase the strength of the composites. When the product layer is rather thick and is composed of brittle intermetallics, the composite itself becomes brittle [30]. In the present work, the sintering temperature was low and the overall exposure of the samples was short for any significant growth of the intermetallic layers to be observed.

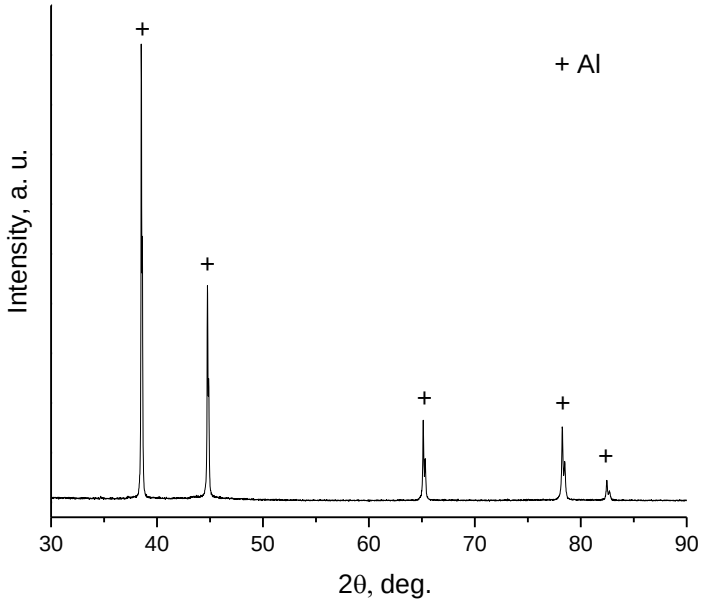

(**a**)

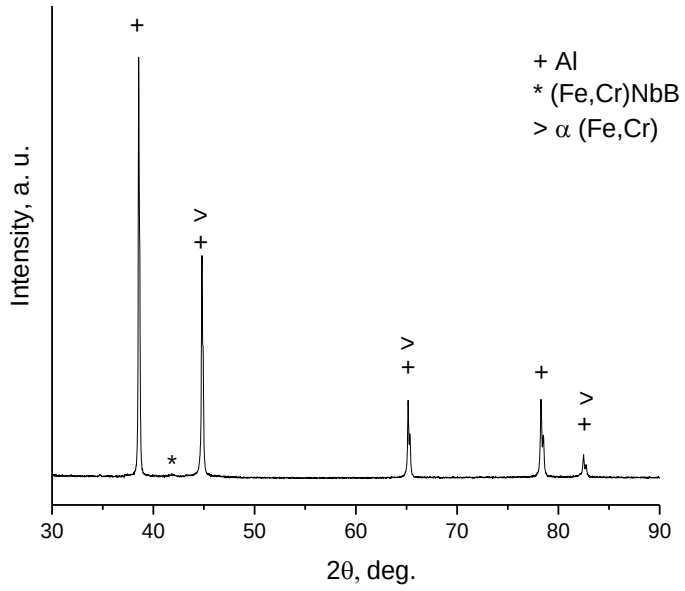

(**b**)

Figure 5. XRD patterns of the hot-pressed composites obtained from (**a**) Al (coarse)–glassy $Fe_{66}Cr_{10}Nb_5B_{19}$ and (**b**) Al (coarse)–crystalline $Fe_{62}Cr_{10}Nb_{12}B_{16}$ mixtures.

Table 1. Relative density of the sintered composites.

Powder	Relative Density, %	
	SPS	HP
Al (coarse)–crystalline $Fe_{62}Cr_{10}Nb_{12}B_{16}$	84 ± 1	78 ± 1
Al (coarse)–glassy $Fe_{66}Cr_{10}Nb_5B_{19}$	99 ± 1	94 ± 1
Al (fine)–crystalline $Fe_{62}Cr_{10}Nb_{12}B_{16}$	94 ± 1	-
Al (fine)–glassy $Fe_{66}Cr_{10}Nb_5B_{19}$	99 ± 1	-

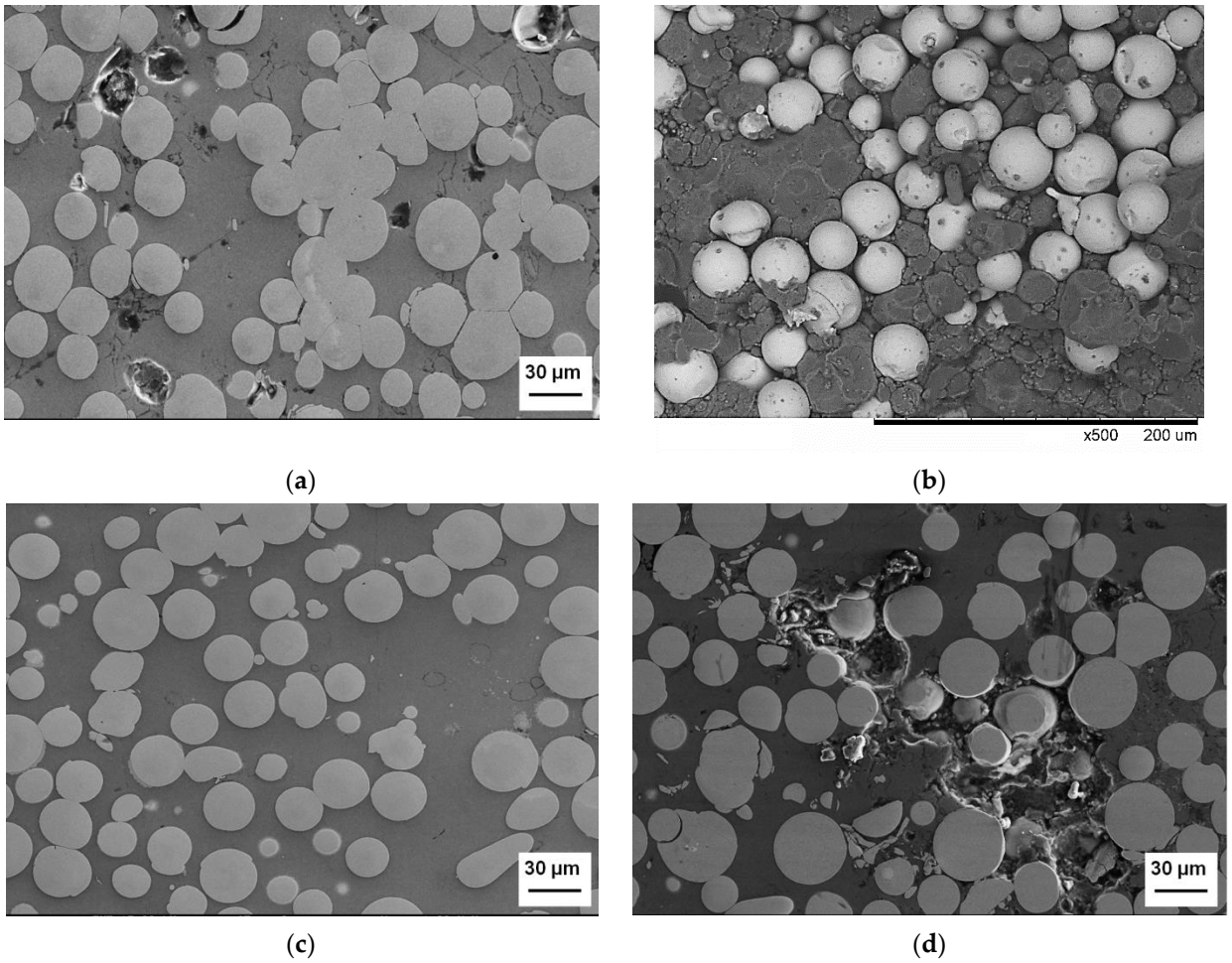

Figure 6. Microstructure of the spark plasma sintered composites obtained from (**a**) Al (coarse)–glassy $Fe_{66}Cr_{10}Nb_5B_{19}$, (**b**) Al (coarse)–crystalline $Fe_{62}Cr_{10}Nb_{12}B_{16}$ mixtures, (**c**) Al (fine)–glassy $Fe_{66}Cr_{10}Nb_5B_{19}$, (**d**) Al (fine)–crystalline $Fe_{62}Cr_{10}Nb_{12}B_{16}$ mixtures. (**a**,**c**,**d**) Micrographs of the polished cross-sections, SE images; (**b**) micrograph of the fracture surface, BSE image.

A combination of a relatively coarse reinforcement and a fine matrix powder provides the best conditions for a homogeneous distribution of the former in the matrix and densification enabled by the matrix [31]. In the present work, composites produced from the fine aluminum particles feature a different distribution pattern of the particles (Figure 6c,d). The tendency of the alloy particles to form chains is significantly reduced. Many alloy particles are fully surrounded by aluminum. This fact can be explained by the particle packing; smaller matrix particles fill the gaps between the reinforcement particles, separating them from each other. The composite containing the crystalline alloy particles has again a higher porosity than the composite with the glassy alloy particles, but this difference in porosity is smaller than in the case of composites formed from the coarse Al powder. The microstructure of the hot-pressed composite (Figure 7) is similar to the microstructure of the composite of the same composition produced by SPS.

In order to reveal the physical nature of the beneficial effect of the glassy state of the alloy for densification during sintering under pressure, model experiments were performed. Fe-based alloys were subjected to SPS under conditions similar to those used for consolidating the Al–Fe-based composites. The recorded temperature and displacement curves are presented in Figure 8. As the glassy $Fe_{66}Cr_{10}Nb_5B_{19}$ alloy is heated above ~490 °C (at this point, the real temperature of the sample can reach T_g), the sample experiences fast shrinkage. At the same temperature, no evidence of shrinkage is observed in the case of the crystalline $Fe_{62}Cr_{10}Nb_{12}B_{16}$. After the experiments, the glassy $Fe_{66}Cr_{10}Nb_5B_{19}$ alloy was a

robust compact (although not fully dense), while the crystalline $Fe_{62}Cr_{10}Nb_{12}B_{16}$ alloy did not experience consolidation, remaining in the powder state.

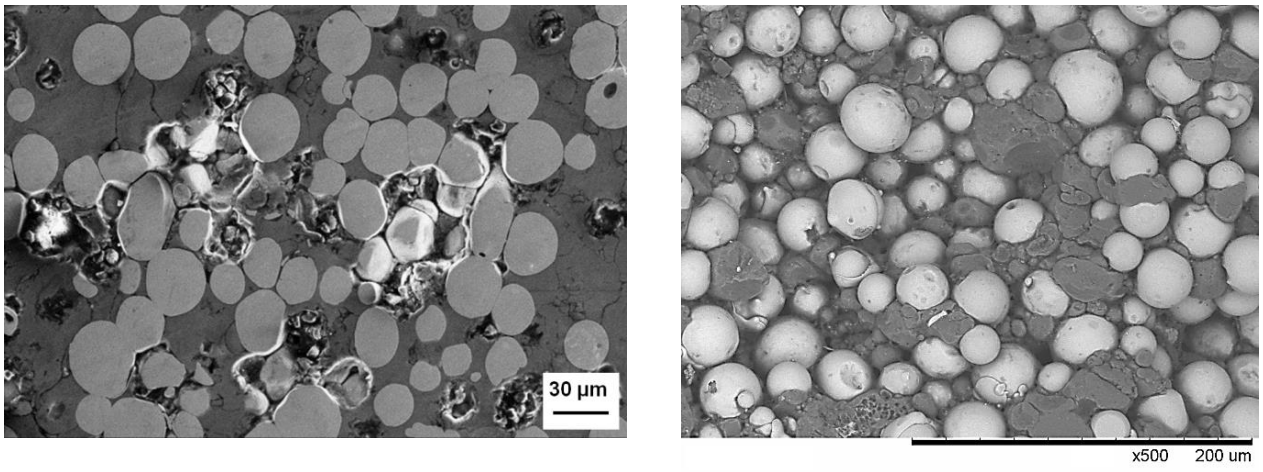

(**a**) (**b**)

Figure 7. Microstructure of the hot-pressed composites obtained from the Al (coarse)–glassy $Fe_{66}Cr_{10}Nb_5B_{19}$ mixture (**a**), Al (coarse)–crystalline $Fe_{62}Cr_{10}Nb_{12}B_{16}$ mixtures (**b**). (**a**) Micrograph of the polished cross-section, SE image; (**b**) micrograph of the fracture surface, BSE image.

Figure 9 shows a schematic of the microstructures of aluminum matrix composites formed using a glassy or a crystalline alloy reinforcement. The glassy state of the reinforcement helps eliminate pores within the particle agglomerates of all sizes thanks to the ability of the metallic glass to flow within its supercooled liquid region. In contrast, the crystalline alloy particles are incapable of deformation at the selected consolidation temperatures.

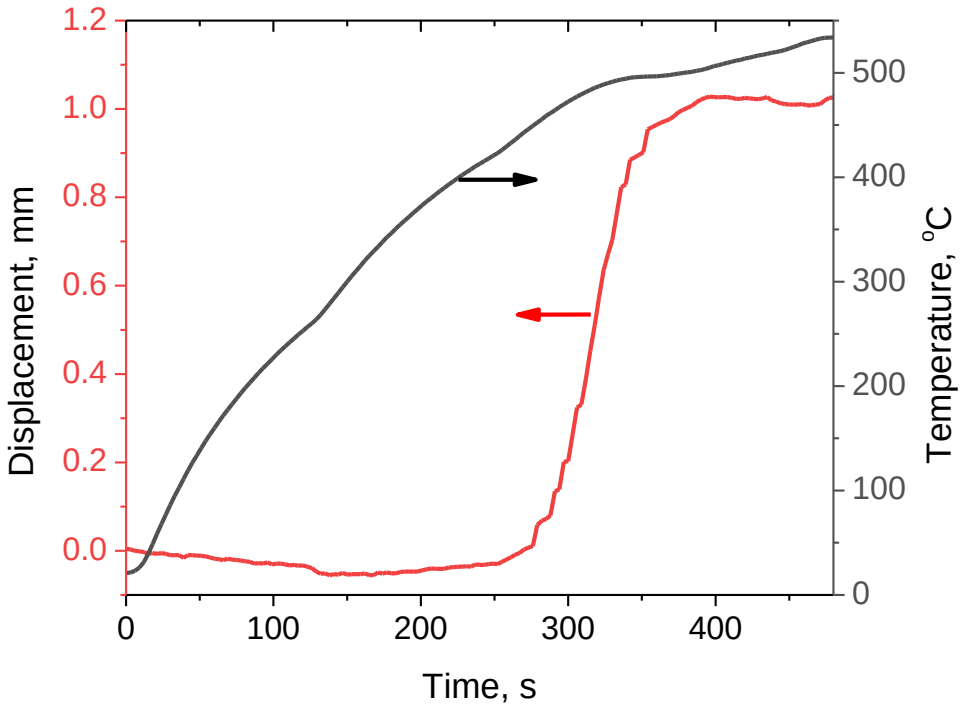

(**a**)

Figure 8. *Cont.*

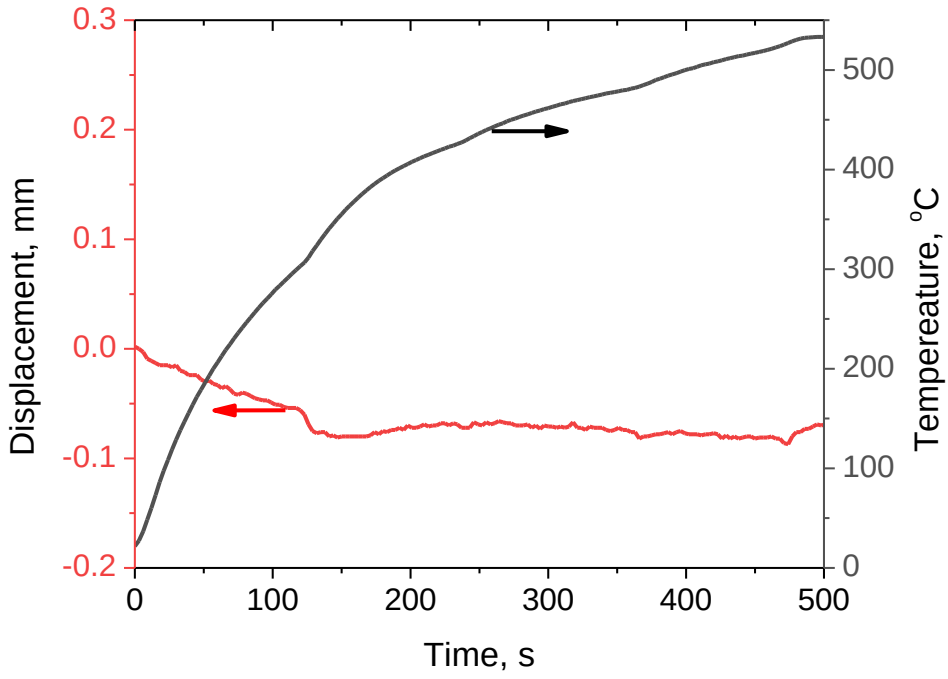

(**b**)

Figure 8. Temperature and displacement versus time during SPS of the glassy $Fe_{66}Cr_{10}Nb_5B_{19}$ (**a**) and crystalline $Fe_{62}Cr_{10}Nb_{12}B_{16}$ (**b**) alloy powders. Black lines, temperature; red lines, displacement.

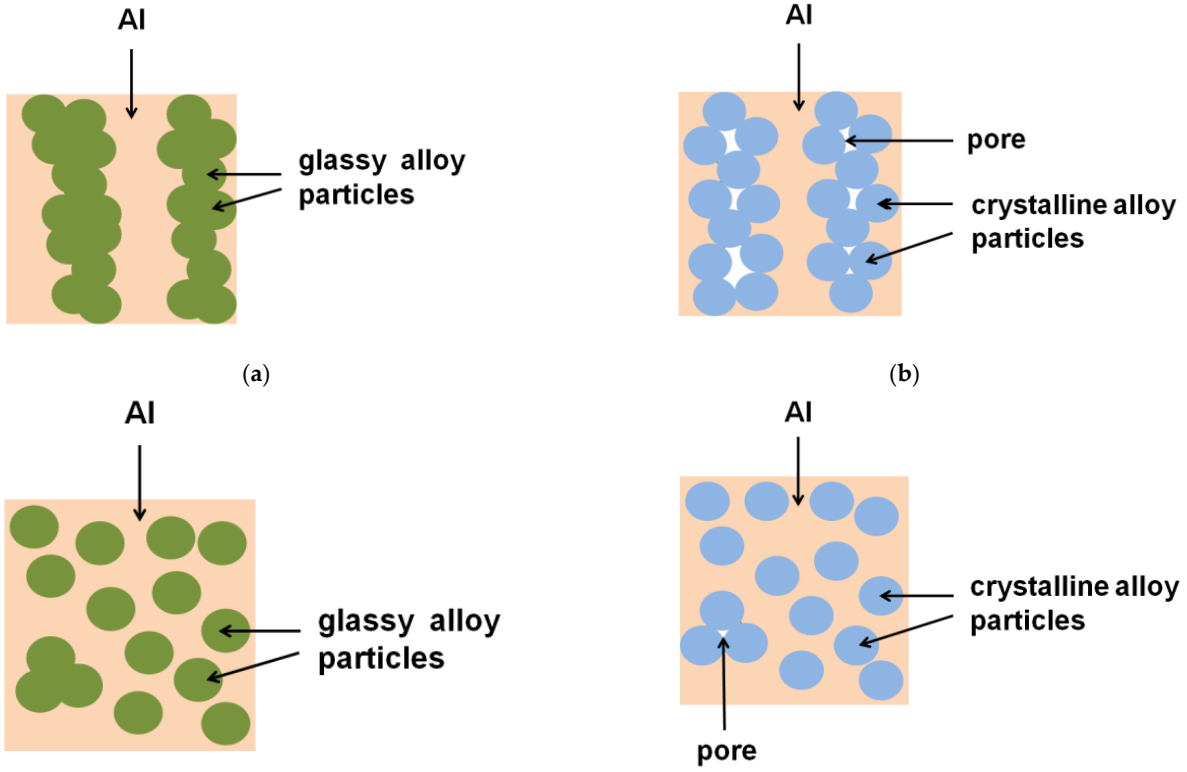

Figure 9. Schematic of the microstructures of aluminum matrix composites formed using a glassy (**a**,**c**) or a crystalline (**b**,**d**) alloy reinforcement.

3.3. Hardness of the Sintered Composites

The Vickers hardness of the composites is presented in Table 2 along with the hardness of the sintered unreinforced aluminum. Due to the high residual porosity, the hardness of the composite obtained from the Al (coarse)–crystalline $Fe_{62}Cr_{10}Nb_{12}B_{16}$ mixture was not measured. It is seen that the hardness of the composites listed in Table 2 is approximately twice the hardness of the unreinforced aluminum. The microhardness of the glassy $Fe_{66}Cr_{10}Nb_5B_{19}$ alloy particles, as determined in ref. [32], is ~1500 $HV_{0.01}$. If the hardness of the corresponding composites had followed the Voigt model, much higher values would have been obtained, close to 50% of the hardness value of the alloy. However, in the microstructures obtained in the present work, the alloy particles (or their chains) are still separated by aluminum, and the formation of a rigid skeletal structure from the alloy particles is prevented. From the above considerations, it follows that Voigt model cannot describe the hardness of composites obtained in the present work.

Table 2. Vickers hardness of the sintered composites and unreinforced aluminum.

Sintered Material	Vickers Hardness, HV_1	
	SPS	HP
Al (coarse)–glassy $Fe_{66}Cr_{10}Nb_5B_{19}$	106 ± 40	83 ± 24
Al (fine)–glassy $Fe_{66}Cr_{10}Nb_5B_{19}$	109 ± 26	-
Al (fine)–crystalline $Fe_{62}Cr_{10}Nb_{12}B_{16}$	72 ± 8	-
Al (fine)	44 ± 1	-

4. Conclusions

The present work clearly demonstrated the benefit of the glassy state of the reinforcing particles for densification of aluminum matrix composites. The consolidation behavior of Al–50 vol.% Fe-based alloy mixtures differing in the size of aluminum particles and crystalline state of the alloy was studied under SPS and HP conditions. Consolidation was carried out by heating the mixtures under pressure above the glass transition temperature of the glassy alloy. When the coarse aluminum powder was used, the particles of the alloys formed chains within the microstructure of the composites. In the composites formed from the fine aluminum particles, the tendency of the Fe-based alloy particles to form chains was diminished and many alloy particles are fully surrounded by aluminum. In both cases, the glassy state of the alloy was beneficial for densification, as the glassy alloy acted as a binder while the crystalline alloy was not capable of performing this task. The binder effect was more pronounced in the case of alloy particles forming chains. The hardness of the composites formed from the Al–50 vol.% glassy $Fe_{66}Cr_{10}Nb_5B_{19}$ mixtures by SPS was found to be twice the hardness of the unreinforced aluminum.

Author Contributions: Conceptualization, D.V.D. and K.G.; methodology, D.V.D.; investigation, V.I.K. and A.V.U.; writing—original draft preparation, V.I.K.; writing—review and editing, D.V.D., G.Y.K. and K.G.; supervision, D.V.D.; funding acquisition, V.I.K. All authors have read and agreed to the published version of the manuscript.

Funding: This research was funded by the Ministry of Science and Higher Education of the Russian Federation, project FWGG-2019-0003.

Conflicts of Interest: The authors declare no conflict of interest.

References

1. Cooke, K. (Ed.) *Aluminium Alloys and Composites*; IntechOpen: London, UK, 2020; 182p.
2. Mavhungu, S.T.; Akinlabi, E.T.; Onitiri, M.A.; Varachia, F.M. Aluminum matrix composites for industrial use: Advances and trends. *Proc. Mmanuf.* **2017**, *7*, 178–182. [CrossRef]
3. Mizuuchi, K.; Inoue, K.; Agari, Y.; Nagaoka, T.; Sugioka, M.; Tanaka, M.; Takeuchi, T.; Tani, J.; Kawahara, M.; Makino, Y.; et al. Processing of Al/SiC composites in continuous solid–liquid co-existent state by SPS and their thermal properties. *Compos. Part B* **2012**, *43*, 2012–2019. [CrossRef]

4. Dash, K.; Chaira, D.; Ray, B.C. Synthesis and characterization of aluminium–alumina micro-and nano-composites by spark plasma sintering. *Mater. Res. Bull.* **2013**, *48*, 2535–2542. [CrossRef]
5. Sweet, G.A.; Brochu, M.; Hexemer, R.L., Jr.; Donaldson, I.W.; Bishop, D.P. Consolidation of aluminum-based metal matrix composites via spark plasma sintering. *Mater. Sci. Eng. A* **2015**, *648*, 123–133. [CrossRef]
6. Liu, Y.; Chen, J.; Wang, X.; Guo, T.; Liu, J. Significantly improving strength and plasticity of Al-based composites by in-situ formed AlCoCrFeNi core-shell structure. *J. Mater. Res. Technol.* **2021**, *15*, 4117–4129. [CrossRef]
7. Lu, T.; Chen, W.; Li, Z.; He, T.; Li, B.; Li, R.; Fu, Z.; Scudino, S. Processing and mechanical properties of fine grained Al matrix composites reinforced with a uniform dispersion of nanocrystalline high-entropy alloy particles. *J. Alloys Compd.* **2019**, *801*, 473–477. [CrossRef]
8. Joseph, A.; Gauthier-Brunet, V.; Joulain, A.; Bonneville, J.; Dubois, S.; Monchoux, J.-P.; Pailloux, F. Mechanical properties of Al/ω-Al-Cu-Fe composites synthesized by the SPS technique. *Mater. Charact.* **2018**, *145*, 644–652. [CrossRef]
9. Wolf, W.; Bolfarini, C.; Kiminami, C.S.; Botta, W.J. Recent developments on fabrication of Al-matrix composites reinforced with quasicrystals: From metastable to conventional processing. *J. Mater. Res.* **2021**, *36*, 281–297. [CrossRef]
10. Inoue, A.; Shen, B.L.; Yavari, A.R.; Greer, A.L. Mechanical properties of Fe-based bulk glassy alloys in Fe–B–Si–Nb and Fe–Ga–P–C–B–Si systems. *J. Mater. Res.* **2003**, *18*, 1487–1492. [CrossRef]
11. Eckert, J.; Das, J.; Pauly, S.; Duhamel, C. Mechanical properties of bulk metallic glasses and composites. *J. Mater. Res.* **2007**, *22*, 285–301. [CrossRef]
12. Gu, X.J.; Poon, S.J.; Shiflet, G.J. Mechanical properties of iron-based bulk metallic glasses. *J. Mater. Res.* **2007**, *22*, 344–351. [CrossRef]
13. Scudino, S.; Surreddi, K.B.; Sager, S.; Sakaliyska, M.; Kim, J.S.; Loser, W.; Eckert, J. Production and mechanical properties of metallic glass-reinforced Al-based metal matrix composites. *J. Mater. Sci.* **2008**, *43*, 4518–4526. [CrossRef]
14. Scudino, S.; Liu, G.; Prashanth, K.G.; Bartusch, B.; Surreddi, K.B.; Murty, B.S.; Eckert, J. Mechanical properties of Al-based metal matrix composites reinforced with Zr-based glassy particles produced by powder metallurgy. *Acta Mater.* **2009**, *56*, 2029–2039. [CrossRef]
15. Dudina, D.V.; Georgarakis, K.; Li, Y.; Aljerf, M.; Braccini, M.; Yavari, A.R.; Inoue, A. Cu-based metallic glass particle additions to significantly improve overall compressive properties of an Al alloy. *Compos. Part A* **2010**, *41*, 1551–1557. [CrossRef]
16. Samanta, A.; Fecht, H.-J.; Manna, I.; Chattopadhyay, P.P. Development of amorphous phase dispersed Al-rich composites by rolling of mechanically alloyed amorphous Al–Ni–Ti powders with pure Al. *Mater. Chem. Phys.* **2007**, *104*, 434–438. [CrossRef]
17. Kotov, A.D.; Mikhaylovskaya, A.V.; Mochugovskiy, A.G.; Medvedeva, S.V.; Bazlov, A.I. Aluminum alloy matrix composite reinforced with metallic glasses particles using hot-roll bonding. *Rus. J. Non-Ferr. Met.* **2020**, *61*, 297–302. [CrossRef]
18. Wang, Z.; Scudino, S.; Stoica, M.; Zhang, W.; Eckert, J. Al-based matrix composites reinforced with short Fe-based metallic glassy fiber. *J. Alloys Compd.* **2015**, *651*, 170–175. [CrossRef]
19. Xie, M.S.; Wang, Z.; Zhang, G.Q.; Yang, C.; Zhang, W.W.; Prashanth, K.G. Microstructure and mechanical property of bimodal-size metallic glass particle-reinforced Al alloy matrix composites. *J. Alloys Compd.* **2020**, *814*, 152317. [CrossRef]
20. Zheng, R.; Yang, H.; Liu, T.; Ameyama, K.; Ma, C. Microstructure and mechanical properties of aluminum alloy matrix composites reinforced with Fe-based metallic glass particles. *Mater. Des.* **2014**, *53*, 512–518. [CrossRef]
21. He, T.; Ertuğrul, O.; Ciftci, N.; Uhlenwinkel, V.; Nielsch, K.; Scudino, S. Effect of particle size ratio on microstructure and mechanical properties of aluminum matrix composites reinforced with $Zr_{48}Cu_{36}Ag_8Al_8$ metallic glass particles. *Mater. Sci. Eng. A* **2019**, *742*, 517–525. [CrossRef]
22. Perriere, L.; Champion, Y. Phases distribution dependent strength in metallic glass–aluminium composites prepared by spark plasma sintering. *Mater. Sci. Eng. A* **2012**, *548*, 112–117. [CrossRef]
23. Wang, Z.; Xie, M.S.; Zhang, W.W.; Yang, C.; Xie, G.Q.; Louzguine-Luzgin, D.V. Achieving super-high strength in an aluminum based composite by reinforcing metallic glassy flakes. *Mater. Lett.* **2020**, *262*, 127059. [CrossRef]
24. Wang, Z.; Georgarakis, K.; Nakayama, K.S.; Li, Y.; Tsarkov, A.A.; Xie, G.; Dudina, D.; Louzguine-Luzgin, D.V.; Yavari, A.R. Microstructure and mechanical behavior of metallic glass fiber-reinforced Al alloy matrix composites. *Sci. Rep.* **2016**, *6*, 24384. [CrossRef] [PubMed]
25. Kuchumova, I.D.; Batraev, I.S.; Ulianitsky, V.Y.; Shtertser, A.A.; Gerasimov, K.B.; Ukhina, A.V.; Bulina, N.V.; Bataev, I.A.; Koga, G.Y.; Guo, Y.; et al. Formation of metallic glass coatings by detonation spraying of a $Fe_{66}Cr_{10}Nb_5B_{19}$ powder. *Metals* **2019**, *9*, 846. [CrossRef]
26. Paul, T.; Singh, A.; Harimkar, S.P. Densification and crystallization in Fe–based bulk amorphous alloy spark plasma sintered in the supercooled liquid region. *Adv. Eng. Mater.* **2017**, *19*, 1700224. [CrossRef]
27. Ertugrul, O.; He, T.; Shahid, R.N.; Scudino, S. Effect of heat treatment on microstructure and mechanical properties of Al 2024 matrix composites reinforced with $Ni_{60}Nb_{40}$ metallic glass particles. *J. Alloys Compd.* **2019**, *808*, 151732. [CrossRef]
28. Guan, H.D.; Li, C.J.; Gao, P.; Prashanth, K.G.; Tan, J.; Eckert, J.; Tao, J.; Yi, J.H. Aluminum matrix composites reinforced with metallic glass particles with core-shell structure. *Mater. Sci. Eng. A.* **2019**, *771*, 138630. [CrossRef]
29. He, T.; Lu, T.; Ciftci, N.; Uhlenwinkel, V.; Chen, W.; Nielsch, K.; Scudino, S. Interfacial characteristics and mechanical asymmetry in Al2024 matrix composites containing Fe-based metallic glass particles. *Mater. Sci. Eng. A* **2020**, *793*, 139971. [CrossRef]

30. Dudina, D.V.; Bokhonov, B.B.; Batraev, I.S.; Kvashnin, V.I.; Legan, M.A.; Novoselov, A.N.; Anisimov, A.G.; Esikov, M.A.; Ukhina, A.V.; Matvienko, A.A.; et al. Microstructure and mechanical properties of composites obtained by spark plasma sintering of Al–$Fe_{66}Cr_{10}Nb_5B_{19}$ metallic glass powder mixtures. *Metals* **2021**, *11*, 1457. [CrossRef]
31. Pines, M.L.; Bruck, H.A. Pressureless sintering of particle-reinforced metal–ceramic composites for functionally graded materials: Part I. Porosity reduction models. *Acta Mater.* **2006**, *54*, 1457–1465. [CrossRef]
32. Dudina, D.V.; Bokhonov, B.B.; Batraev, I.S.; Amirastanov, Y.N.; Ukhina, A.V.; Kuchumova, I.D.; Legan, M.A.; Novoselov, A.N.; Gerasimov, K.B.; Bataev, I.A.; et al. Interaction between $Fe_{66}Cr_{10}Nb_5B_{19}$ metallic glass and aluminum during spark plasma sintering. *Mater. Sci. Eng. A* **2021**, *799*, 140165. [CrossRef]